Macromolecules
ARTICLE

Macromolecules **2010**, *43*, 3399–3405 **3399**
DOI: 10.1021/ma1000157

Morphology Evolution of Spin-Coated Films of Poly(thiophene−phenylene−thiophene) and [6,6]-Phenyl-C_{71}-butyric Acid Methyl Ester by Solvent Effect

Shu-Hua Chan,[†,‡] Yu-Sheng Hsiao,[†] Ling-I Hung,[†] Gue-Wuu Hwang,[†] Hsin-Lung Chen,[‡] Ching Ting,*[,†] and Chih-Ping Chen*[,†]

[†]*Materials and Chemical Laboratories, Industrial Technology Research Institute, 195, Sec. 4, Chung Hsing Road, Chutung, Hsinchu 310, Taiwan, and* [‡]*Department of Chemical Engineering, National Tsing Hua University, Hsin-Chu 30013, Taiwan*

Received January 6, 2010; Revised Manuscript Received March 1, 2010

ABSTRACT: This paper describes the influence of the solvent on the morphological evolution and performance of polymer solar cells (PSCs) based on blended films of poly(thiophene−phenylene−thiophene) and [6,6]-phenyl-C_{71}-butyric acid methyl ester ($PC_{71}BM$). The blends are spin-coated with solvents exhibiting various evaporation rates, including *o*-dichlorobenzene (DCB), chlorobenzene (CB), chloroform (CF), and tetralin. The changing morphologies of these blended films are monitored using atomic force microscopy (AFM) and transmission electron microscopy (TEM). A solvent having a higher boiling point [1,8-octanedithiol (OT)] is also introduced as an additive to further fine-tune the morphology of the bulk heterojunction (BHJ). We demonstrate herein that the morphology of a blend—and, hence, the performance of a BHJ device—can be manipulated by controlling the rate of solvent evaporation during film formation. The resulted fine-scale phase separation leads to enhanced performance of such organic photovoltaic devices. The highest power efficiency for our PSCs (5.8%, AM 1.5G irradiation (100 mW/cm^2)) resulted when we use DCB as the solvent with OT as a processing additive.

Introduction

Because of the low weight, flexibility, and large-area throughput characteristics, polymer solar cells (PSCs) prepared from thin films of conjugated polymer blends are being actively researched;[1−7] to date, their power conversion efficiencies (PCEs) have reached as high as 7.9% by Solarmer.[8] Typically, a conjugated polymer behaving as an electron donor (D) is blended with an electron acceptor (A), usually a fullerene, to achieve a bulk heterojunction (BHJ) structure. The polymer plays the key roles of absorbing light, creating excitons for subsequent charge separation, and transporting holes to the anode. Further improvements in device performance will require materials harvesting more light from the solar flux[9−11] and the development of well-defined morphologies to allow effective charge separation and transport. The blended D and A materials require a nanomorphology in which they provide suitable interfaces for exciton dissociation. Furthermore, the D and A units must segregate into size domains that are homogeneous on the order of the exciton diffusion length. In the meantime, they must form a nanoscale interpenetrating phase possessing continuous paths between the electrodes for efficient charge transport.

Because the photoactive layers are typically deposited through spin-casting, thermodynamic as well as kinetic effects determine their morphologies.[12] From a thermodynamic point of view, the intrinsic properties of the components of the solution (the D/A materials and the solvent) used to deposit the blend film, such as the Flory−Huggins parameter, the ratio, interactions, and solubility of the D and A materials, play key roles during the evolution of the film's morphology.[8] During the film formation process, kinetic factors, such as the solvent evaporation rate and the post-treatment and crystallization behavior, have significant effects on the morphology of the active layer. Several approaches have been reported to effectively control this morphology and, hence, improve the performance of PSCs.[13−17] In 2005, Li et al. reported the beneficial effect of solvent annealing, raising the PCE of the P3HT:PCBM cell to 4.4%.[13] The performance can also increased up to 5% through thermal annealing.[14] Varying the composition of the solvent mixture is another promising route to improve device performance.[10,15−17] Adding higher boiling point solvent [e.g., nitrobenzene or 1,8-octanedithiol (OT)] to a typical casting solution [e.g., in chlorobenzene (CB) or *o*-dichlorobenzene (DCB)], allows further control over the final device morphology and performance. For example, this fabrication protocol has resulted in a PCE of 5.5% for a device based on poly[2,6-(4,4-bis(2-ethylhexyl)-4*H*-cyclopenta[2,1-*b*;3,4-*b*]dithiophene)-*alt*-4,7-(2,1,3-benzothiadiazole)] (PCPDTBT).[10] The addition of OT to poly(3-hexylthiophene) (P3HT):[6,6]-phenyl-C_{61}-butyric acid methyl ester ($PC_{61}BM$) or PCPDTBT:$PC_{71}BM$ mixtures can induce preferential domains of the PCBM and prolong the plasticization of the photoactive layer, thereby allowing structural reorganization to take place.

In a previous study, we synthesized a new class of conjugated polymer featuring coplanar thiophene−phenylene−thiophene (TPT) units; we found that poly(TPT) derivatives possess high field effect hole mobilities (ca. 10^{-3} cm^2/(V s)) and promising PSC performance (4.3% under AM 1.5 G).[9,18] The performance of devices based on poly(TPT)s was limited, however, by not yet optimized control over their morphologies. Herein we present a comparative study of the morphological evolution of PTPTBT/$PC_{71}BM$-based solar cell devices (Figure 1) incorporating blends that were spin-coated from

*Corresponding author: e-mail chihping_chen@itri.org.tw (C.-P.C.), cting@itri.org.tw (C.T.); Tel 886-35-913588; Fax 886-35-827694.

Published on Web 03/12/2010

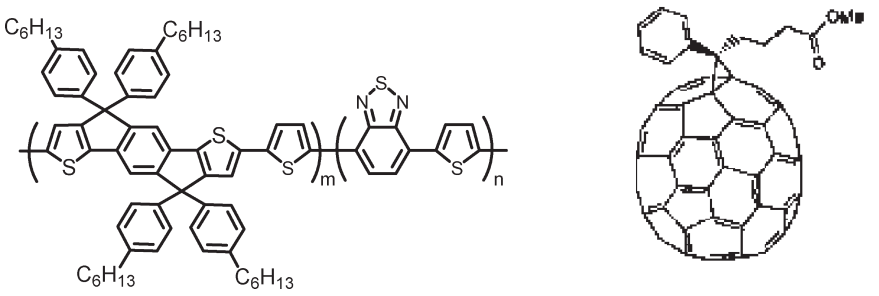

Figure 1. Chemical structures of PTPTBT and $PC_{71}BM$.

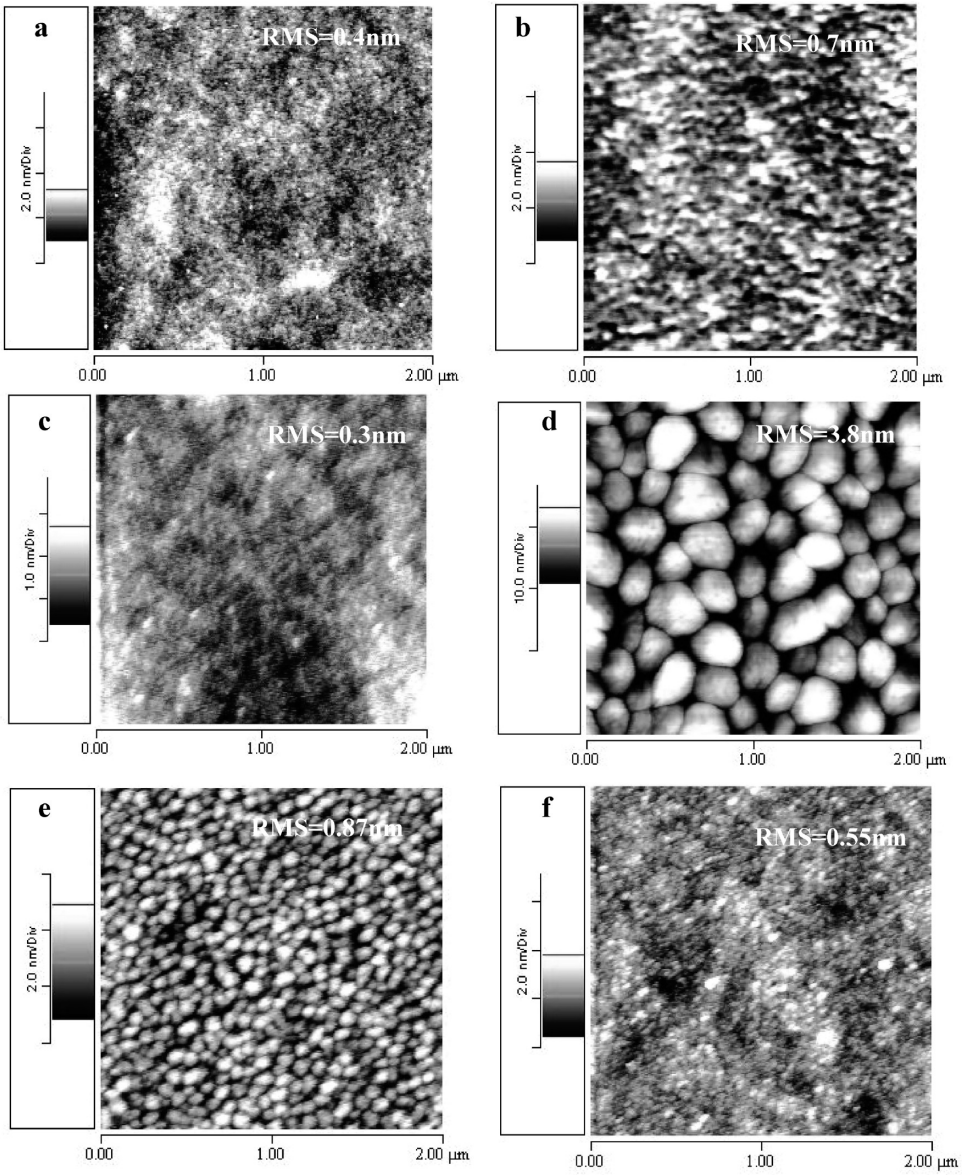

Figure 2. Tapping-mode AFM topographic images obtained from the surfaces of PTPTBT:$PC_{71}BM$ films; (a−d) prepared from the blend films (1:3) using (a) DCB, (b) CB, (c) tetralin, and (d) CF as solvents; (e, f) CF-derived films prepared at PTPTBT:$PC_{71}BM$ ratios (e) 1:2 and (f) 1:1.

solvents [DCB, CB, CF, and tetralin] possessing a range of boiling points. An even high boiling point solvent is added as an additive to verify the correlation of solvent effect/solvent quality and morphology. The relationship between morphologies and the device performance was examined using tapping-mode AFM and TEM. In this paper we describe the relationship between the morphology and the PCE as the feasibility of controlling the morphologies of newly designed conjugated polymers.

Results and Discussion

Morphologies Evolution by Solvent Effect. We prepared mixed solutions by dissolving PTPTBT and $PC_{71}BM$ in the desired solvents and continuously stirring them in dark

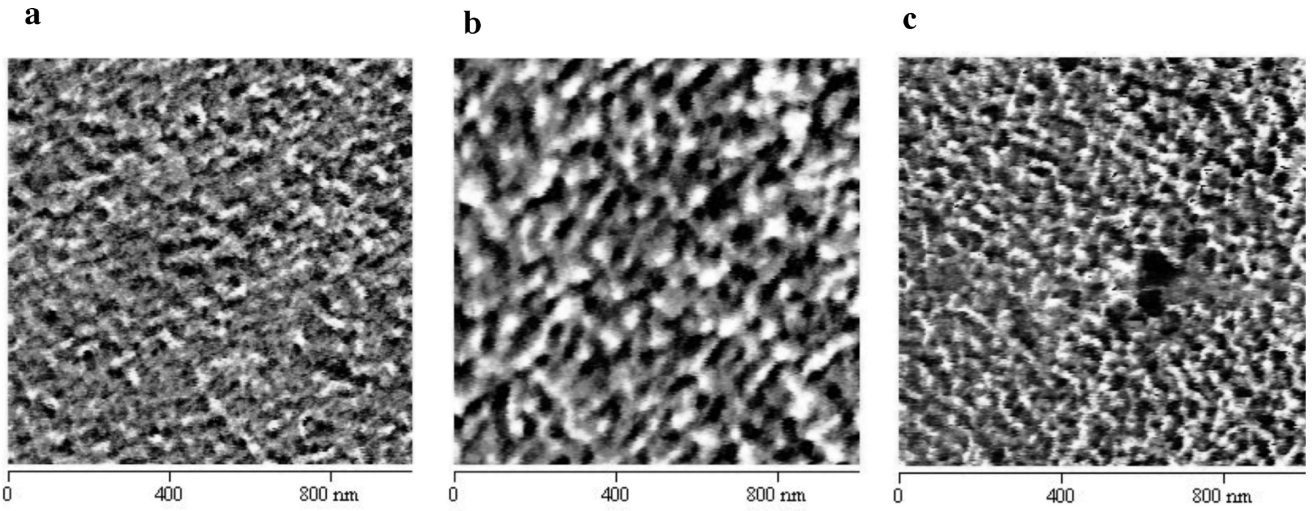

Figure 3. Phase images of PTPTBT:$PC_{71}BM$ (1:3) films prepared using (a) DCB, (b) CB, and (c) tetralin as solvents.

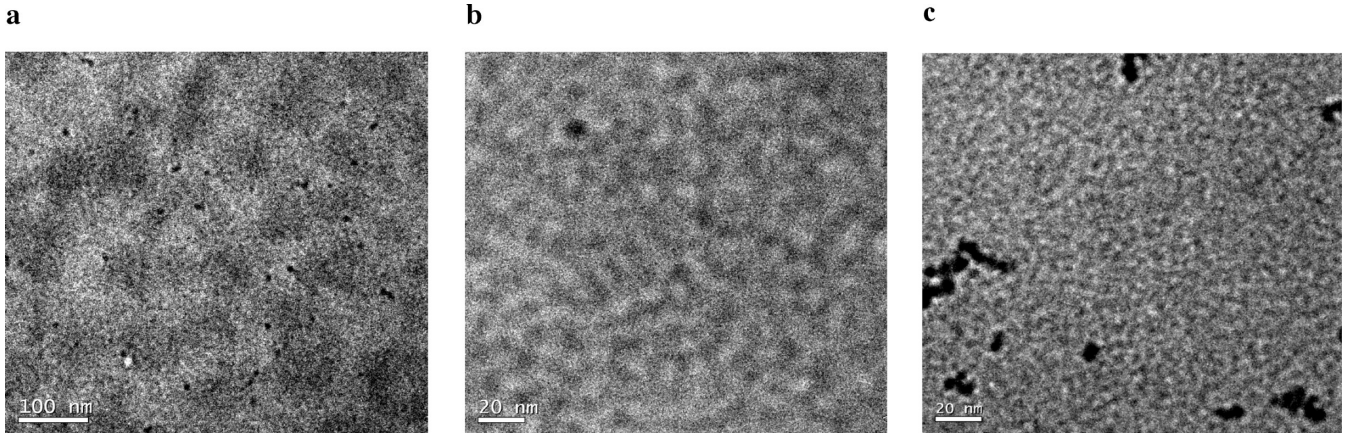

Figure 4. TEM images of PTPTBT:$PC_{71}BM$ films spin-cast from the solvents (a) CF, (b) DCB, and (c) DCB/1.25% OT.

overnight. To investigate how the morphologies of the PTPTBT:$PC_{71}BM$ films evolved over time, we employed AFM in the tapping mode to characterize their topographies. For direct comparison, we prepared the films for AFM analysis under the same conditions used for device fabrication. Figure 2 displays the topographies of PTPTBT:$PC_{71}BM$ (1:3) layers spin-coated from DCB, CB, CF, and tetralin. Larger aggregates and, thus, blend phase separation occurred only for the CF sample (Figure 2d). The morphology in the blend film changed dramatically upon changing the solvent. For high-boiling-point solvents (DCB, CB, tetralin), the thin films of PTPTBT:$PC_{71}BM$ incorporating 75 wt % PCBM were rather flat and featureless. The root-mean-squared (rms) surface roughnesses of these films were less than 1 nm. The surface of the corresponding CF sample was significantly rougher, with an rms roughness of 3.8 nm, and it featured an island-like morphology (diameter: ca. 300 nm). Figure 2d−f reveals that the rms surface roughness increased and the island formation became clearly evident upon increasing the PCBM content in the blend from 1:1 to 1:3. This result can be explained primarily by considering that the kinetics of phase segregation is influenced by the limited solubility and crystallization of PCBM.[19] When a thin film is prepared from a blend by spin-coating a solution, the solvent evaporates quickly and an equilibrium state is rarely reached. Typically, PCBM crystals precipitate when the PCBM concentration reaches its equilibrium solubility limit. Because the composition of the liquid phase of the CF system reached its equilibrium solubility limit of PCBM faster, larger scale of PCBM aggregates resulted, especially at higher PCBM contents. Similar results have been observed for polyfluorene copolymer and poly[2-methoxy-5-(3,7-dimethyloctyloxy)-1,4-phenylenevinylene] (MDMO−PPV) blend systems.[19,20]

Phase images of two-component blend film provide clues regarding the surface hardness and the identity of the fullerene- and polymer-rich domains.[17] The phase image in Figure 3a reveals two distinct feature types in the DCB film: a dark-colored agglomerate, which we attribute to PCBM-rich domains, and bright regions, denoting the PTPTBT-rich domains. The width of elongated PCBM domain had dimensions of ca. 20 nm. Although the DCB and CB films possessed similar topographic characteristics, their magnified phase images reveal several variations. For example, CB (Figure 3b) induced a larger phase separation, characterized by segregation of elongated larger PCBM-rich domains (length $>$ 50 nm) surrounded by continuous PTPTBT-rich phase. The phase image of the tetralin sample was similar to that of the DCB sample, with a PCBM domain size of ca. 20 nm (Figure 3c). The phase images suggest that the main morphological feature of the blend films prepared from high-boiling-point solvents was a homogeneous distribution of the two components within the nanoscale. Nevertheless, morphological changes are difficult to observe in tapping-mode

AFM images because the phase image signal is affected by several factors, including tip feature and the surface properties of the active layer.[21] Therefore, we also conducted TEM experiments to confirm these morphologies. Figure 4a displays a TEM image of a PTPTBT:$PC_{71}BM$ thin film sample incorporating 66 wt % PCBM, prepared from CF. We attribute the dark areas to the PCBM domains because the electron scattering density of PCBM is greater than that of the conjugated polymer.[22] This image reveals a morphology in which PCBM-rich domains (ca. 100 nm) are dispersed within a PTPTBT-rich matrix. Comparisons with AFM images confirmed that the island-like regions corresponded to PCBM-rich domains, the sizes of which increased upon increasing the PCBM content. The morphology of the DCB sample in Figure 4b features nanoscale phase separation with a domains size of ca. 20 nm, consistent with the AFM images.

Photovoltaic Properties. We fabricated organic photovoltaic devices (OPVs) having the layered configuration glass/indium tin oxide (ITO)/poly(3,4-ethylenedioxythiophene):poly(styrenesulfonate) (PEDOT:PSS)/PTPTBT:PCBM/Ca/Al using methods similar to those we reported previously.[9,18] The layers of Ca (30 nm) and Al (100 nm) were deposited thermally under vacuum. The optimal thickness of the active layers obtained under these conditions was ca. 90 nm. After encapsulation using UV-curing glue, we measured the $I-V$ characteristics in air. Table 1 and Figure 5 display the output characteristics of the devices prepared under various fabrication conditions. The DCB- and tetralin-derived cells exhibited similar AM 1.5G PCEs of ca. 4.2%, whereas the CB-derived device exhibited slightly poorer value of ca. 3.7%. The nearly identical performances of the DCB- and tetralin-derived devices were due primarily to their similar degrees of nanophase separation, as indicated in their AFM phase images. The relatively lower PCE of the CB-derived device appears to be related to its larger phase separation domains (> 50 nm), which provided smaller interfacial areas for exciton dissociation; as a result, its current density decreased by ca. 15%. The PCE of the CF-derived device was significantly lower than those of the others, as a result of remarkable decreases in its current density and fill factor (FF). We also recorded the PL (photoluminescence) behavior of respective films. The PL of the PTPTBT film lies near the yellow region with an emission peak at 576 nm and is completely quenched for all determined blend films (Figure S1). This result indicates that photoinduced charge transfer from the polymer to PCBM is observed even for the CF-derived device. Poor OPV performance for polymer:PCBM blends is drastically associated with larger scale phase separation. This hypothesis is reasonable; for shorter exciton diffusion lengths (< 20 nm), free carrier generation will be limited by large fullerene clusters (200−500 nm) and, thereby, cause unsatisfactory performance.

Thermal annealing of the P3HT system generally results in enhanced degrees of crystallinity, improved nanoscale morphologies, and, consequently, improved device performances.[16] In general, the annealing temperature was set around the thermal transition of the polymers. The PTPTBT, being an amorphous polymer, does not have observable thermal transitions below the degradation point. Such behavior has, however, not been observed for PTPTBT or most other newly synthesized conjugated polymers.[8,10,23] Apart from the judicious use of various appropriate solvents, strategies based on slow drying of spin-coated films or solvent vapor annealing of blends have been eliminated as means toward improving device performance in this polymer system. Because the morphologies of our PTPTBT-based active layers were directly influenced by the rates of solvent evaporation

Table 1. Characteristic Current−Voltage Parameters for Devices Tested under Standard AM 1.5G Conditions

sample	J_{sc} (mA/cm^2)	V_{oc} (V)	FF	PCE (%)
CF	5.8	0.84	0.41	2
CB	8.4	0.81	0.54	3.7
DCB	10.1	0.80	0.53	4.3
tetralin	9.8	0.81	0.53	4.2
DCB/OT	10.7	0.85	0.64	5.8

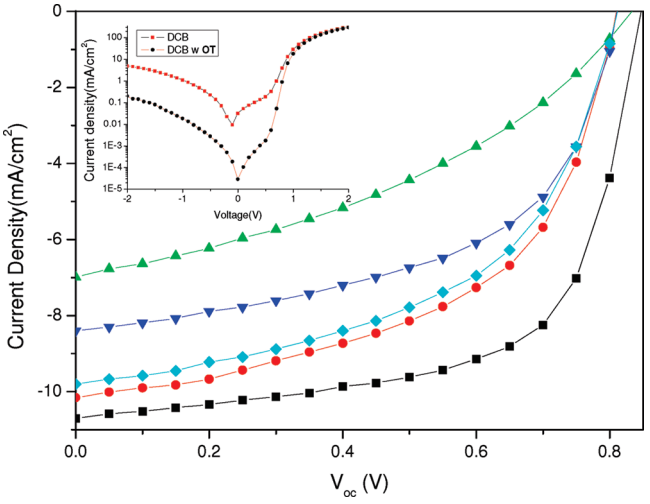

Figure 5. Current density−potential characteristics of PTPTBT/PCBM PSC devices under illumination with AM 1.5G simulated solar light (100 mW/cm^2): DCB/1.25% OT (■), DCB (●), CF (▲), CB (▼), and tetralin (◆). Inset: current density−potential characteristics of the DCB and DCB/OT devices in the dark.

of the cast blends, we investigated the effect of using a mixed solvent system (DCB/OT) to manipulate the BHJ morphology directly during the film formation process. In addition, OT has preferred solubility of the fullerene component; the PCBM tends to remain in solution longer than the polymer, thereby enabling control over the miscibility between the two components and phase separation of the BHJ.[16] We varied the solvent ratios (OT concentration from 0 to 1.75 vol %) as well as the composition and concentration of the active layer solutions (PTPTBT-to-PCBM ratios from 1:1.5 to 1:4) while monitoring the resulting morphologies; optimization of this process was determined qualitatively from the $I-V$ characteristics (see Figure S2 in the Supporting Information). A steady rise and a subsequent fall in efficiency occurred upon increasing the OT concentration; the value of V_{oc} remained almost constant, but that of J_{sc} followed the PCE trend. The FFs increased upon increasing the concentration of OT. We monitored the effect of the PTPTBT-to-PCBM ratio at the optimized OT concentration (1.25 vol %). Figure S2b reveals that the optimal PTPTBT-to-PCBM ratios fell within the range from 1:3 to 1:3.7 (w/w). Lower contents of PCBM (< 75 wt %) led to inefficient electron/hole separation because of inappropriate morphologies.[5] Upon increasing the PCBM content, the values of both J_{sc} and the FF increased in the mixed solvent-derived devices. Our most efficient device was fabricated using a polymer concentration of 10 mg/mL, a spin rate of 2000 rpm for 30 s, and DCB as the solvent incorporating OT as the additive at 1.25 vol %. This device exhibited a PCE of 5.8% under AM 1.5G irradiation (100 mW/cm^2), with values of J_{sc}, V_{oc}, and FF of 10.7 mA/cm^2, 0.85 V, and 0.64, respectively. The PCEs of these DCB/OT-fabricated devices were reproducible, with a variation of only 10% exhibited among five individual PSC devices. The performance of this polymer OPV device is among the highest

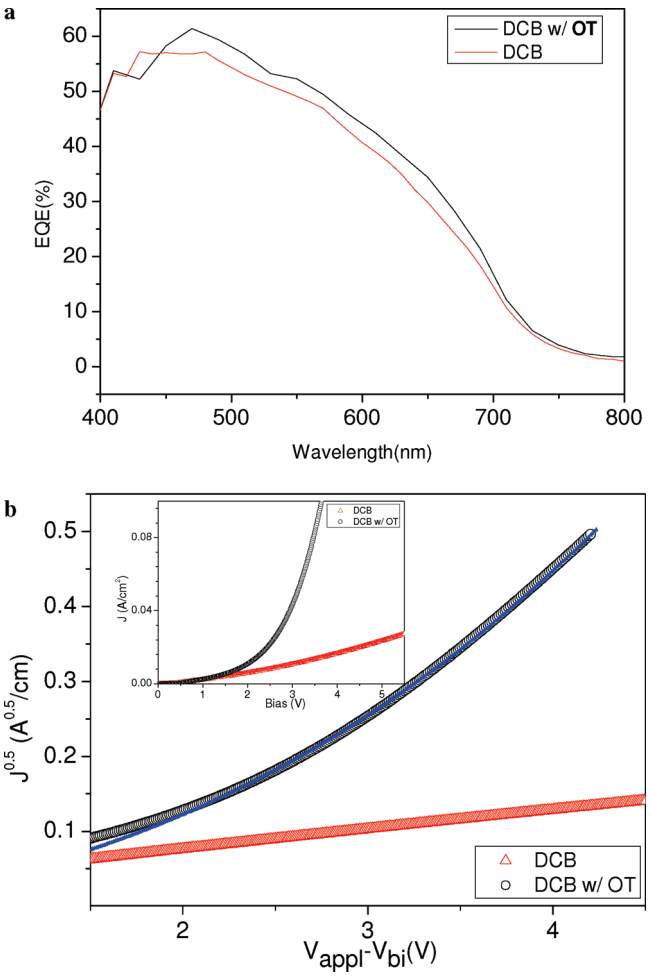

Figure 6. (a) EQE spectra of devices prepared from DCB and DCB/OT. (b) $J^{0.5}-V$ plots for hole-only devices incorporating the DCB- and DCB/OT-derived blend films (red and black lines, respectively). The blue line was fitted using the field-dependent SCLC equation. Inset: $J-V$ plot prior to correction of the voltage.

ever reported. In comparison with the DCB-fabricated device, the FF underwent a significant increase of ca. 20%, whereas the values of J_{sc} and V_{oc} increased only slightly. Figure 5 indicates that the DCB/OT-derived device exhibited a high rectification ratio due to its lower dark current and higher shunt resistance. We calculated the series resistance (R_s) and shunt resistance (R_{sh}) from the inverse slope of the $J-V$ curve. A small decrease of R_s from 6.9 to 6.6 Ω cm^2 is observed after using the OT additive, which implies the bulk resistance of devices is similar. A significant increase of R_{sh} from 294 to 585 Ω cm^2 is obtained, which indicates the defects caused charge recombination and leakage current is lower for DCB/OT device. The interfacial organization at the junction and spatial distribution of two components may contribute to the performance enhancement. The effects of additives have been noted previously by Heeger et al. and Yang et al. when using PCPDTBT and P3HT as donor materials, respectively.[15,16] They found the presence of OT improved the packing of the polymers, thereby leading to optimized morphologies. Figure 6a compares the external quantum efficiency (EQE) spectra of our DCB and DCB/OT devices, we observe contributions to the EQE at wavelengths between 400 and 700 nm, with the maximum EQEs being ca. 56% and 61% at 470 nm, respectively. Convolution of the spectral response with the photon flux AM 1.5G spectrum (100 mW/cm^2) gives an estimate for the J_{sc} under irradiation. The calculated J_{sc} for DCB- and DCB/OT-derived devices are 8.9 and 9.5 mA/cm^2, respectively. Because of the mismatch between EQE and photon flux AM 1.5, there are ~10% discrepancy between convolution and solar simulator data. The EQE response curves of the DCB- and DCB/OT-derived devices were nearly identical, except that the response intensity of the latter was slightly higher. The same phenomena are evident in the corresponding UV−vis spectra (Figure S3). As a result, we can eliminate the notion that better packing of the polymers results in a red shift in the UV−vis spectra in our system.

Determining Hole Mobility from SCLC Transistor Characteristics. To determine whether the hole mobility was affected by the presence of the additive, we fabricated hole-only devices using a high-work-function material, palladium (Pd), as the cathode to block the back injection of electrons. When a sufficient voltage is applied to this hole-only device, the transport of holes through the polymer film is limited by the space charge that accumulates. The space charge limited current (SCLC) is described by the equation

$$J = \frac{9}{8}\varepsilon_r\varepsilon_0\mu_h\frac{V^2}{L^3}$$

where ε_r is the dielectric constant of the polymer, ε_0 is the permittivity of free space, μ_h is the hole mobility, V is the voltage applied to the device, and L is the polymer thickness.[24,25] Figure 6b displays the experimental dark-current densities of the DCB- and DCB/OT-derived devices measured in the hole-only devices. The applied voltage was corrected for the built-in voltage (V_{BI}), which we estimated from the difference between the work function and the energy level of the highest occupied molecular orbital (HOMO) of PTPTBT. The plot of $J^{0.5}$ with respect to V for the DCB-derived device was a straight line; from the slope we calculated the field-independent mobility to be 2.2×10^{-6} cm^2/(V s). The hole mobility of the DCB/OT-derived device was field-dependent; its mobility followed the equation

$$\mu_h = \mu_{h0}e^{\gamma\sqrt{V/L}}$$

where μ_{h0} is the zero-field mobility and γ is the field dependence prefactor; the carrier mobility was estimated from the equation[26]

$$J = \frac{9}{8}\varepsilon_r\varepsilon_0\mu_{h0}e^{0.89\gamma\sqrt{V/L}}\frac{V^2}{L^3}$$

We used this equation to fit the $J^{0.5}-V$ curve data for the DCB/OT-derived device to obtain values for the zero-field hole mobility and field-dependent prefactor of 1.1×10^{-6} cm^2/(V s) and 7.9×10^{-4} (m/V)$^{1/2}$. Thus, the hole mobility did not improve upon the use of OT as the additive.

To confirm our hypothesis of a correlation existing between the morphology and the performance, we recorded TEM and AFM images of the morphology of the active layer processed using OT. The DCB/OT film was rather flat (rms was ca. 0.6 nm), and the phase image features nanoscaled phase separation (Figure S4). Figure 4c reveals a well-defined blend of acceptor materials (PCBM-rich domains; grain size < 15 nm) surrounded by PTPTBT domains. The TEM images of the DCB and DCB/OT films (Figure 4, b and c, respectively) reveal similar morphologies, although the PCBM domains in the latter film were smaller and better separated. We suspect that it was the differing grain sizes that caused the variations in device performance.[27] The TEM image reveal that the DCB/OT film contained well-connected PTBTBT networks and larger D/A interfaces with

interpenetrating networks (IPNs). Overall, these morphological and electronic features suggest that the improved PCE was due primarily to spatial distribution of the D/A domains, rather than the enhanced hole mobility exhibited in the case of the P3HT/PCBM blend.[15] Smaller domain sizes provide larger D/A interfaces, thereby increasing the probability of exciton dissociation and, thus, avoiding wasteful recombination pathways. The number of photogenerated charges is enhanced at a smaller-scale phase separation; therefore, we observed higher values of J_{sc}. Furthermore, well-defined IPN structures ensure continuous pathways for both charges to reach their appropriate electrodes, thereby providing higher FF values.

Conclusions

One key aspect toward high-performance devices of a newly synthesized conjugated polymer is the detailed knowledge on morphology−property relations of blends. As for the optimization of PTPTBT device performance, we dedicated 3 months endeavor to understand the entangled effects of solvent selection, composition of the solutions, blend film preparation details, and post-treatment. We used several processing solvents to compare the morphologies (observed using AFM and TEM) of PTPTBT/PCBM blend films as active layers in OPV devices. When using OT as an additive in DCB as the solvent, the PCE reached 5.8% mainly due to the remarkable increase in the FF. TEM analyses revealed that small donor and acceptor domains were formed directly during the spin-coating process, thereby providing an optimal IPN network and improved performance. The optimized morphology featured with appropriate nanoscale regimes allows the photogenerated excitons being sufficiently close to the interfaces for successful charge generation and with continuous percolating pathways for better carrier transport. This study highlights the importance of examining the internal structures of newly synthesized conjugated polymers to fully understand the effects of various processing conditions on their morphologies and, thereby, their contributions toward high-performance PSCs.

Experimental Section

Materials and Equipment. All chemicals were purchased from Aldrich and used as received unless otherwise specified. PTPTBT was synthesized according to procedures described previously.[9] Absorption spectra were recorded using a Perkin-Elmer Lambda 950 UV−vis spectrophotometer. The morphologies of the polymer films were analyzed using a VEECO DICP-II atomic force microscope operated in the dynamic force mode at ambient temperature and an etched Si probe operated under a resonant frequency of 131 kHz and a spring constant of 11 N/m. Samples for the TEM analysis were prepared by spin-casting from various blend solutions onto a PEODOT:PSS/glass substrate. The films were then floated onto water and placed on a 200-mesh carbon-coated Cu TEM grid (Agar Sci., Inc.). TEM images were recorded using a JEOL-2010 transmission electron microscope and an internal charge-coupled device (CCD) camera. $I-V$ curves of the PSC devices were measured using a computer-controlled Keithley 2400 source measurement unit (SMU) equipped with a Peccell solar simulator under AM 1.5G illumination (100 mW/cm^2). The illumination intensity was calibrated using a standard Si photodiode detector equipped with a KG-5 filter. The output photocurrent was adjusted to match the photocurrent of the Si reference cell to obtain a power density of 100 mW/cm^2. The efficiency of 3.5% of a P3HT/PCBM reference cell measured under illumination in our laboratory was verified to be 3.4% under AM 1.5G conditions (100 mW/cm^2) at the National Institute of Advanced Industrial Science and Technology (AIST, Japan). After encapsulation, all device measurements were performed in an ambient atmosphere at 25 °C.

Photovoltaic Cell Fabrication and Testing. All bulk-heterojunction PV cells were prepared using the following device fabrication procedure.[28] Glass/ITO substrates [Sanyo, Japan (8 Ω/□)] were sequentially patterned lithographically, cleaned with detergent, ultrasonicated in acetone and isopropyl alcohol, dried on a hot plate at 120 °C for 5 min, and treated with oxygen plasma for 5 min. PEDOT:PSS (Baytron P-VP AI4083) was passed through a 0.45 μm filter prior to being deposited on ITO at a thickness of ca. 30 nm through spin-coating at 3000 rpm in air; the sample was then dried at 150 °C for 30 min inside a glovebox. A blend of PTPTBT and 1-(3-methoxycarbonyl)propyl-1-phenyl-[6,6]-C_{71} ($PC_{71}BM$) [1:3 (w/w), 7.5 mg/mL in various solvent] was stirred overnight, filtered through a 0.2 μm poly(tetrafluoroethylene) (PTFE) filter, and then spin-coated (500−2000 rpm, 30 s) on top of the PEDOT:PSS layer. The device was completed by depositing a 30 nm thick layer of Ca and a 100 nm thick layer of Al at pressures of less than 10^{-6} Torr. The active area of the device was 4 mm^2. Finally, the cell was encapsulated using UV-curing glue (Nagase, Japan).

Acknowledgment. We thank the Ministry of Economic Affairs, Taiwan, for financial support.

Supporting Information Available: PL, UV-vis and AFM images. This material is available free of charge via the Internet at http://pubs.acs.org.

References and Notes

(1) Thompson, B. C.; Fréchet, J. M. J. *Angew. Chem., Int. Ed.* **2008**, *47*, 58.
(2) Dennler, G.; Scharber, M. C.; Brabec, C. J. *Adv. Mater.* **2009**, *21*, 1323.
(3) Krebs, F. C. *Sol. Energy Mater. Sol. Cells* **2009**, *93*, 394.
(4) Helgesen, M.; Søndergaard, R.; Krebs, F. C. *J. Mater. Chem.* **2010**, *20*, 36.
(5) Krebs, F. C.; Gevorgyan, S. A.; Alstrup, J. *J. Mater. Chem.* **2009**, *19*, 5442.
(6) Krebs, F. C. *Org. Electron.* **2009**, *10*, 761.
(7) Park, S. H.; Roy, A.; Beaupré, S.; Cho, S.; Coates, N.; Moon, J. S.; Moses, D.; Leclerc, M.; Lee, K.; Heeger, A. J. *Nat. Photonics* **2009**, *3*, 297.
(8) Chen, Y.; Hou, J.; Zhang, S.; Liang, Y.; Yang, G.; Yang, Y.; Yu, L.; Wu, Y.; Li, G. *Nat. Photonics* **2009**, *3*, 649.
(9) Chen, C. P.; Chan, S. H.; Chao, T. C.; Ting, C.; Ko, B. T. *J. Am. Chem. Soc.* **2008**, *130*, 12828.
(10) Peet, J.; Kim, J. Y.; Coates, N. E.; Ma, W. L.; Moses, D.; Heeger, A. J.; Bazan, G. C. *Nat. Mater.* **2007**, *6*, 497.
(11) Spanggaard, H.; Krebs, F. C. *Sol. Energy Mater. Sol. Cells* **2004**, *83*, 125.
(12) Yang, X.; Loos, J. *Macromolecules* **2007**, *40*, 1353.
(13) Li, G.; Shrotriya, V.; Huang, J.; Yao, Y.; Moriarty, T.; Kmery, K.; Yang, Y. *Nat. Mater.* **2005**, *4*, 864.
(14) Ma, W. L.; Yang, C. Y.; Gong, X.; Lee, K.; Heeger, A. J. *Adv. Funct. Mater.* **2005**, *15*, 1617.
(15) Yao, Y.; Hou, J.; Xu, Z.; Li, G.; Yang, Y. *Adv. Funct. Mater.* **2008**, *18*, 1783.
(16) Lee, J. K.; Ma, W. L.; Brabec, C. J.; Yuen, J.; Moon, J. S.; Kim, J. Y.; Lee, K.; Bazan, G. C.; Heeger, A. J. *J. Am. Chem. Soc.* **2008**, *130*, 3619.
(17) Moulé, A. J.; Meerholz, K. *Adv. Mater.* **2008**, *20*, 240.
(18) Yu, C. Y.; Chen, C. P.; Chan, S. H.; Hwang, G. W.; Ting, C. *Chem. Mater.* **2009**, *21*, 3262.
(19) Nilsson, S.; Bernasik, A.; Budkowski, A.; Moons, E. *Macromolecules* **2007**, *40*, 8291.
(20) Hoppe, H.; Sariciftci, N. S. *J. Mater. Chem.* **2006**, *16*, 45.
(21) Crispin, X.; Jakobsson, F. L. E.; Crispin, A.; Grim, P. C. M.; Andersson, P.; Volodin, A.; van Haesendonck, C.; van der Auweraer, M.; Salaneck, W. R.; Berggren, M. *Chem. Mater.* **2006**, *18*, 4354.
(22) Yang, X.; van Duren, J. K. J.; Janssen, R. A. J.; Michels, M. A. J.; Loos, J. *Macromolecules* **2004**, *37*, 2151.

(23) Shi, C.; Yao, Y.; Yang, Y.; Pei, Q. *J. Am. Chem. Soc.* **2006**, *128*, 8980.
(24) Reid, O. G.; Munechika, K.; Ginger, D. S. *Nano Lett.* **2008**, *8*, 1602.
(25) Melzer, C.; Koop, E. J.; Mihailetchi, V. D.; Blom, P. W. M. *Adv. Funct. Mater.* **2004**, *14*, 865.
(26) Goh, C.; Kline, R. J.; McGehee, M. D.; Kadnikova, E. N.; Frechet, J. M. J. *Appl. Phys. Lett.* **2005**, *86*, 3.
(27) Dante, M.; Garcia, A.; Nguyen, T.-Q. *J. Phys. Chem. C* **2009**, *113*, 1596.
(28) Chan, S.-H.; Chen, C.-P.; Chao, T.-C.; Ting, C.; Ko, B.-T. *Macromolecules* **2008**, *41*, 5519.